INSTRUMENTATION AND MEASUREMENT

A spin-based magnetic scanning microscope for *in-situ* strain tuning of soft matter

Zhe Ding(丁哲)[1,2], Yumeng Sun(孙豫蒙)[1,2], Mengqi Wang(王孟祺)[1,2], Pei Yu(余佩)[1,2], Ningchong Zheng(郑宁冲)[3,4,5,6], Yipeng Zang(臧一鹏)[3,4,5,6], Pengfei Wang(王鹏飞)[1,2,7], Ya Wang(王亚)[1,2,7], Yuefeng Nie(聂越峰)[3,4,5,6], Fazhan Shi(石发展)[1,2,7,8,†], and Jiangfeng Du(杜江峰)[1,2,7,‡]

[1] *CAS Key Laboratory of Microscale Magnetic Resonance and School of Physical Sciences, University of Science and Technology of China, Hefei* 230026, *China*

[2] *CAS Center for Excellence in Quantum Information and Quantum Physics, University of Science and Technology of China, Hefei* 230026, *China*

[3] *National Laboratory of Solid State Microstructures, Nanjing University, Nanjing* 210093, *China*

[4] *Jiangsu Key Laboratory of Artificial Functional Materials, Nanjing University, Nanjing* 210093, *China*

[5] *College of Engineering and Applied Science, Nanjing University, Nanjing* 210093, *China*

[6] *Collaborative Innovation Center of Advanced Microstructures, Nanjing University, Nanjing* 210093, *China*

[7] *Hefei National Laboratory, University of Science and Technology of China, Hefei* 230088, *China*

[8] *School of Biomedical Engineering and Suzhou Institute for Advanced Research, University of Science and Technology of China, Suzhou* 215123, *China*

(Received 17 December 2022; revised manuscript received 8 February 2023; accepted manuscript online 10 February 2023)

We present a magnetic scanning microscope equipped with a nitrogen-vacancy (NV) center scanning probe that has the ability to mechanically tune the strain of soft matter *in-situ*. The construction of the microscope and a continuous strain-tuning sample holder are discussed. An optically detected magnetic resonance protocol utilized in the imaging is described. In order to show the reliability of this microscope, the strain conduction is estimated with finite element simulation, and x-ray diffraction is required for calibration when freestanding crystal films are under consideration. A magnetic imaging result is displayed to demonstrate the nano-scale imaging capability. The microscope presented in this work is helpful in studying strain-coupled magnetic physics such as magnetic phase transition under strain and strain-tuned cycloidal orientation tilting.

Keywords: nitrogen-vacancy (NV) center, antiferromagnetism, strain tuning, soft matter

PACS: 75.50.–y, 75.75.–c, 07.79.–v, 42.50.Dv **DOI:** 10.1088/1674-1056/acbaee

1. Introduction

As a novel quantum sensor, nitrogen-vacancy color centers (NV center) in diamond have high magnetic sensitivity ($\sim 1\ \mu T/Hz^{1/2}$ for DC and $\sim 1\ nT/Hz^{1/2}$ for AC), high spatial resolution (~ 10 nm)[1–3] and ability to work under ambient condition.[4] Because of the merits above, it has been used in scanning imaging of ferromagnets,[5] antiferromagnets,[6–8] skyrmions[9–11] and two-dimensional (2D) materials.[12–14]

Soft-matter science has been intensively studied as an emergent field of condensed matter physics. Subjects in soft-matter science such as far-from-equilibrium dynamics, self-assembly, and jamming are broadly connected to biology, chemistry, and other areas.[15] Recently, the soft matters are utilized to efficiently tune strain in freestanding films because of their low elastic moduli and high ability to bear deformations.[16,17] Because of its rich physical content, multiple experimental techniques have been applied to acquire different kinds of information from soft matter. For example, diffusing wave spectroscopy, high-speed confocal microscopy, holographic microscopy, x-ray tomography, and neutron scattering have been applied to acquire structural data of soft matter.[15] NV centers have also been utilized to probe phase transitions in a soft matter as NMR sensors.[18] However, a magnetic microscope with nano-scale resolution and capability to *in-situ* tuning soft matter has not been built. Such a microscope is useful in the analysis of soft matter microstructure,[18–20] designing functional materials,[21,22] tuning novel condensed matter materials,[16,17,23] etc.

Towards such a microscope, we construct a scanning NV microscope (SNVM) combining functions including magnetic resonance, optical excitation, nano-scale scanning, and *in-situ* strain tuning. The capability of strain tuning is estimated with finite element simulation and x-ray diffraction (XRD) experiments are required to calibrate strain conduction when freestanding crystal films are studied. A demonstration of nano-scale magnetic imaging is also displayed in this paper.

2. Implementation

2.1. Overview

In this work, we build an SNVM that can adjust the strain of soft matter *in-situ*. A sketch of the microscope which utilizes a single NV as the scanning probe is shown in Fig. 1.

†Corresponding author. E-mail: fzshi@ustc.edu.cn

‡Corresponding author. E-mail: djf@ustc.edu.cn

© 2023 Chinese Physical Society and IOP Publishing Ltd

As shown in the inset, an NV center is constructed by a nitrogen atom replacing a carbon site and an adjacent vacancy in the diamond. To realize near-field scanning, atomic force microscopy (AFM) is adopted in this system. The diamond probe with an NV center at its apex is assembled through a glass beam to a quartz tuning fork force sensor which provides a feedback signal for the AFM controlling system (refer to Subsection 2.2).[24] An objective is utilized to focus a green laser on the NV center and collect fluorescent photons. To lift the degeneracy between electronic spin states $|m_S = \pm 1\rangle$ of NV centers, a permanent magnet whose position is adjusted by a three-axis actuator is equipped. In order to perform magnetic resonant operations, microwave (MW) is emitted by a suspended antenna.

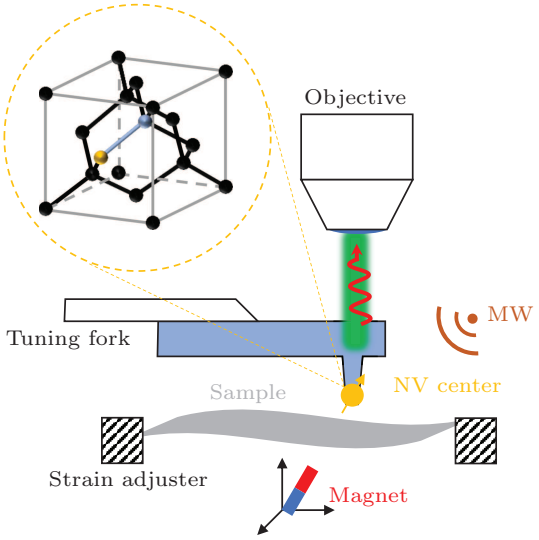


Fig. 1. Principle sketch of the microscope. A diamond probe (blue) with an NV center at the tip (orange) is assembled with a tuning fork. The structure of an NV center is shown in the inset. MW (brown) and laser (green) are applied to the NV center and fluorescence (red) is collected by an objective. A soft-matter sample is installed on the strain adjuster which can mechanically tune the strain applied to the sample.

Both ends of the soft matter sample are fixed to the strain adjuster with epoxy and a linear actuator is employed to adjust the distance between the two ends and apply stress to the sample. By measuring the change of length ΔL and the original length L, one can define a nominal strain

$$\varepsilon_n = \frac{\Delta L}{L} \times 100\%. \tag{1}$$

This value is often used to characterize the macroscopic deformation of organic materials.[16,17,23]

2.2. Peripheral equipments

The scheme of the microscope is displayed in Fig. 2, microwave bridge, and electrical units are used to control the microscope head and acquire data. A home-built confocal microscope is applied to polarize the spin state of the NV center and read out its final spin state. A fiber-based laser diode (CIQTEK GYPFL 520-10) emits a green laser which is coupled into free space by a fiber port (Thorlabs PAF2P-18A). The fluorescence transmits through a dichroic mirror (Thorlabs DMLP567L), a spatial filter, and a band pass filter, then to an avalanche photodiode (Excelitas SPCM-AQRH). The electrical pulse generated by the photodiode is transmitted to a counter card (NI PCIe-6612). A CMOS (Thorlabs DCC1645C) based home-built optical microscope is coupled to the confocal setup with two beam splitters (Thorlabs BP245B1). By using the optical microscope, one can easily align the sample, probe, and MW antenna. MW generated by a source (Rigol DSG3065G) is amplified (Minicircuits ZHL-16W-43-S+) and finally fed to the NV probe with a micro antenna. A pulse generator (Spincore Pulseblaster ESR-PRO) is equipped to synchronize lasers, MW pulses, and the counter card.

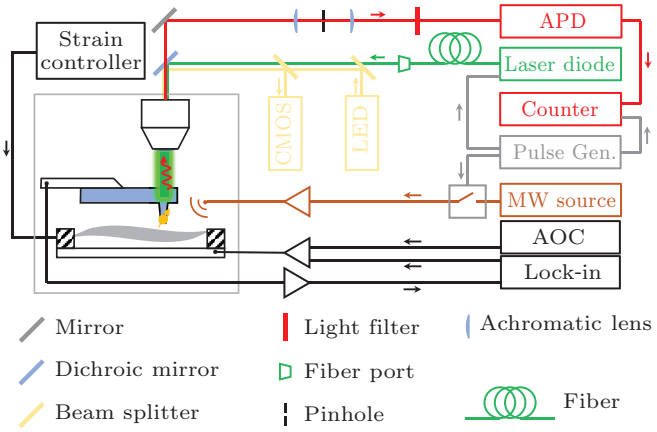


Fig. 2. Scheme of the microscope. A green laser for optical pumping is generated by the laser diode (green) and the fluorescence is detected by an APD (red) and finally fed to a counter card (red). A CMOS-based optical microscope (yellow) is coupled to the confocal microscope. MW applied to the NV center is generated by an MW source (brown). A pulse generator (grey) synchronizes the laser, MW pulse, and the counter card. Electric voltages generated by the AOC and lock-in are amplified by a voltage amplifier and fed to the AFM scanner. The strain controller is connected to the strain adjuster which actuates the *in-situ* strain tuning with an electric sawtooth wave.

The AFM controlling system is composed of a lock-in amplifier (ZI MFLI), an analog output card (AOC, NI PCIe-6704), and a charge amplifier (FEMTO HQA-15M-10T). The electronic signal from the tuning fork is amplified by the charge amplifier and fed into the lock-in amplifier. A built-in feedback loop of the lock-in generates an electrical voltage that controls the Z axis of the AFM scanner. The AOC is programmed with scanning coordinates and controls the X and Y axes of the AFM scanner.

The strain adjuster is equipped with a linear actuator (MultiFields Linear25-Sim) and remote, *in-situ* strain tuning is enabled via the strain controller connected to the actuator.

2.3. Microscope head

By combining a probe stage, a sample stage, and an MW stage to a rigid steel pedestal, we build a multi-degree-of-freedom, high-stability microscope head which is displayed

in Fig. 3(a). A confocal image of NV probes on one micro diamond chip is acquired by scanning the objective with a nano-scanner (PI P-516.3CD, not shown in the figure), the image is shown in Fig. 3(c). After calibration of all the NV probes, only one with the longest coherence time and high count rate is reserved while other probes are broken with a micro-manipulator to guarantee good contact between the NV probe and the sample. Besides, a three-axis linear actuator (PI M-122.2DD, not shown in the figure) is installed below the microscope head to adjust the magnetic field applied to the sample.

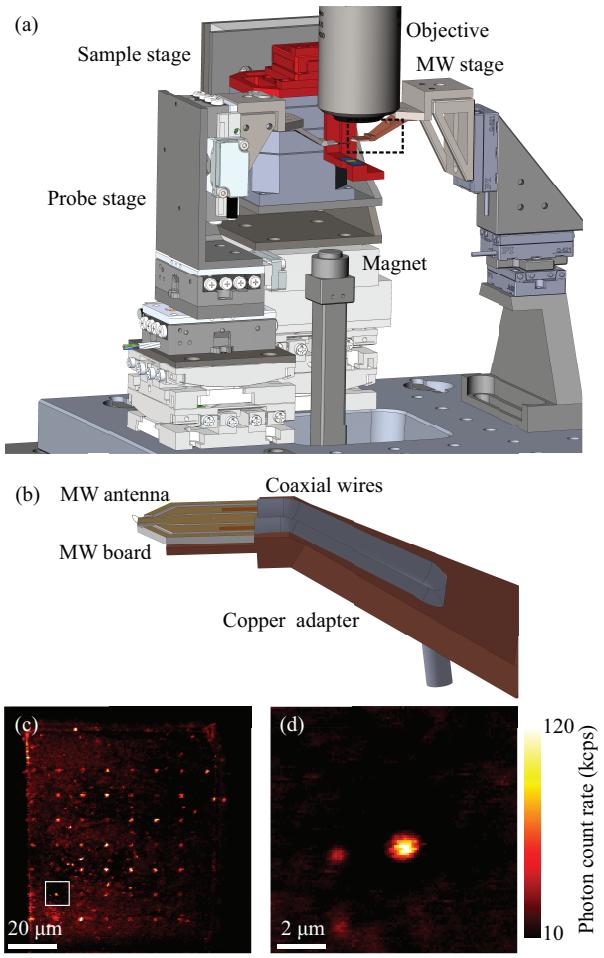


Fig. 3. (a) Structure of the microscope head. A probe stage (equipped with a three-axis actuator with μm resolution), a sample stage (equipped with a three-axis actuator with μm resolution and a three-axis scanner with nm resolution), and an MW stage (equipped with a three-axis actuator) are assembled to one steel pedestal. The sample holder with strain tuning ability is highlighted in red. The MW antenna is in the dashed box, the detailed structure is shown in (b). (b) Detailed structure of the MW antenna. The antenna is bonded to the MW board and the coaxial wires are soldered to the board to transport the MW pulses. Be aware, in order to show the detailed structure, (b) is in an upside-down configuration. (c) Confocal image of a diamond probe. A detailed image of the NV (marked with a white box on the left side) used in the experiment is shown in (d).

The probe and the sample stage are both able to realize three-dimensional position adjustment (Micronix PPS-28). To ensure contact between the probe and sample, a set of goniometers (Micronix PG-50) with two degrees of freedom is installed in the sample stage. The MW stage is constructed by a set of three-axis linear actuators (PI Q-521). During experiments, the AFM scanner (COREMORROW P63.XYZ-D1) installed to the sample stack realizes magnetic imaging by scanning the sample in a nano-scale.

Highlighted in Fig. 3 with red, mounted to the AFM scanner is the sample holder equipped with the strain adjuster mentioned in Subsection 2.2. Such a sample holder can tune the deformation of a soft matter sample by mechanically stretching two ends and adjusting ΔL in Eq. (1). Since a displacement sensor with sub-micrometer sensitivity is built into the actuator, fine strain tuning is enabled.

In published works, resonant MW could be emitted by a copper wire spanned on the sample,[24] a co-planar waveguide[25] or a micro antenna fabricated on the sample.[6] Since soft matter normally possesses the ability to realize high deformations, MW radiation structures mentioned above may be destroyed during strain tuning. To solve this problem, we fabricate a suspended antenna, shown in Fig. 3(b). The antenna is bonded to the front end of the MW board while coaxial wires transporting MW are soldered to the rear end. The board is soldered to the copper adapter, which is fixed to the MW stage. The MW stage is composed of three actuators (PI Q-521), which enables a three-dimensional position adjustment of the antenna. Since the antenna is not directly engaged with the sample, it holds still during strain tuning and the MW radiated to the NV center keeps steady even though the sample experiences large deformations.

2.4. Dual-iso-B detection

Continuous wave protocol (CW) based on optically detected magnetic resonance (ODMR) is often utilized to realize the detection of static magnetic signals.[26] The corresponding energy level transitions are shown in Fig. 4(a). After being pumped into the phonon sideband by a green laser, the NV electron relaxes into the excited state with spin conserved. This transition from the excited state to the ground state is correlated to the spin state while $|m_S = \pm 1\rangle$ has a higher possibility to relax through singlet state $^1A_1$ during which no photon is emitted. And $|m_S = 0\rangle$ has a higher possibility to jump into the ground state and emit a fluorescence photon. Because of this difference, the spin state can be read by counting the fluorescent photons of an NV center.

In the CW process, optical pumping and spin resonant driving are performed simultaneously while the population of $|m_S = 0\rangle$ in the equilibrium state determines the readout signal. By collecting photon counts under different MW frequencies, a CW spectrum may be acquired as shown in Fig. 4(b). The spectrum is composed of two Lorentzian peaks because of the hyperfine coupling to the intrinsic ^{15}N nuclear spin of the NV center:

$$S(f,B_{\rm p}) = -\frac{A}{(f-f_+(B_{\rm p}))^2/\Delta^2+1} - \frac{A}{(f-f_-(B_{\rm p}))^2/\Delta^2+1}, \quad (2)$$

where $B_{\rm p}$ is the external magnetic field's projection to the NV axis, Δ is the width of one Lorentzian peak, and positions of both Lorentzian peaks $f_\pm(B_{\rm p}) = D - \gamma_{\rm e} B_{\rm p} \pm A_{\rm N}/2$. Noting that the zero-field splitting of an NV center $D = 2870$ MHz, electron gyromagnetic ratio $\gamma = 2.8$ MHz/Gauss, hyperfine coupling strength $A_{\rm N} = 3.03$ MHz are all known, generally, one can acquire $B_{\rm p}$ by fitting a CW spectrum to Eq. (2).

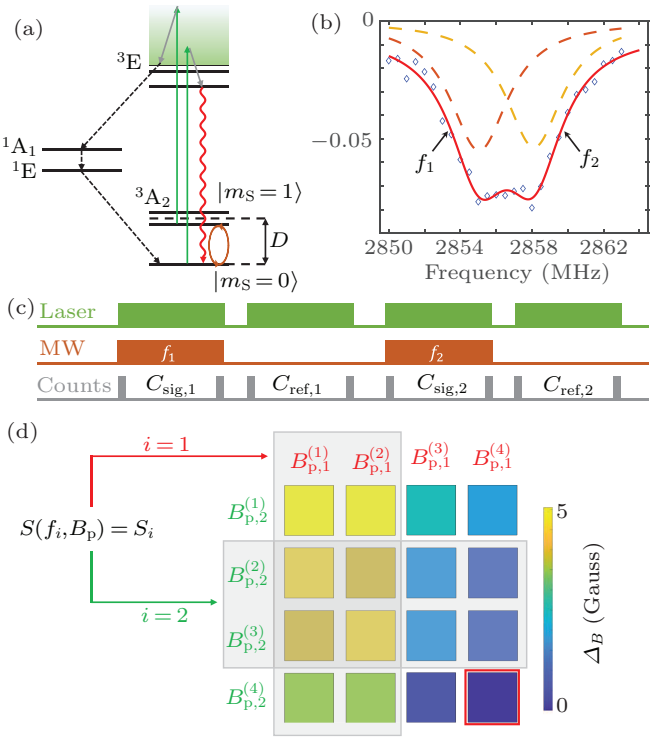


Fig. 4. Principle of the dual-iso-B protocol. (a) Energy levels of an NV center. Green arrows are optical pumping transitions, black dotted arrows are the inter-system crossing transitions and the red wavy arrow is the optical transition that emits a fluorescence photon. The brown circular arrow is the spin resonance driven by MW. (b) A CW spectrum. Experimental data are shown in blue diamonds and the red curve is the Lorentzian fitting result. Lorentzian curves of two nuclear spin states are shown with dashed curves. (c) Pulse sequence of the dual-iso-B protocol. (d) Scheme of solving $B_{\rm p}$. By solving equations ($i = 1,2$), two sets of solutions $(B_{\rm p,1}^{(m)}, B_{\rm p,2}^{(n)})$ $(m,n = 1,2,3,4)$ are acquired. Differences $\Delta_{B,mn}$ between solutions in different sets are plotted. Complex solutions are abandoned and covered with grey boxes while real solutions are compared. Solutions with the smallest difference (highlighted with a red box) are employed as the physical solutions.

In a scanning experiment, for the sake of scanning speed, we adopt the dual-iso-B protocol.[6,23] The pulse sequence of this protocol is shown in Fig. 4(c). According to such protocol, ODMR under two MW frequencies f_1 and f_2 are detected, and the signal of such a detection is defined to qualitatively characterize the magnetic texture:

$$\alpha = \frac{S(f_1,B_{\rm p}) - S(f_2,B_{\rm p})}{S(f_1,B_{\rm p}) + S(f_2,B_{\rm p})}, \quad (3)$$

in which the signal under each frequency is defined by $S_i = (C_{{\rm sig},i} - C_{{\rm ref},i})/C_{{\rm ref},i}, \quad i \in \{1,2\}$. Besides, as shown in Fig. 4(d), one can solve $B_{\rm p}$ by constructing a set of equations:

$$S(f_i,B_{\rm p}) = S_i, \quad i \in \{1,2\}. \quad (4)$$

Be aware that each equation is a quartic algebraic equation, so it may have up to four real solutions, the j-th solution of equation-i is written as $B_{{\rm p},i}^{(j)}$. One cannot determine the physical solution from plural solutions with only one equation, but by comparing solution sets of two equations, the correct physical solution is found.[23] Specifically, as shown in Fig. 4(d), we calculate differences

$$\Delta_{B,mn} = |B_{\rm p,1}^{(m)} - B_{\rm p,2}^{(n)}|$$

of solutions of different equations and find the smallest Δ_{B,m^*n^*}. Then $B_{\rm p,1}^{(m^*)}$ and $B_{\rm p,2}^{(n^*)}$ are determined to be physical solutions. Since two equations correspond to two independent measurements to the same $B_{\rm p}$, the average value of both physical solutions from two equations, $(B_{\rm p,1}^{(m^*)} + B_{\rm p,2}^{(n^*)})/2$, is adopted as the result.

3. Results

3.1. Strain characterization

As an example for testing the setup, we investigate the strain distribution on organic soft matter and its conduction onto a freestanding $BiFeO_3$ film. The soft matter sample we used is polyethylene naphthalate (PEN) while the freestanding film is prepared with molecular beam epitaxy (MBE) and assembled to the PEN substrate with epoxy. To estimate the strain distribution on PEN, we use finite element software (COMSOL) to calculate the stationary solution of its solid mechanics model. And XRD experiments could be utilized to calibrate the strain of the BFO film.

In the finite element simulation, according to the sample used in our experiment, a 12 mm×5 mm×0.1 mm PEN ribbon is considered. Since the left and right margins of the PEN's bottom surface are assembled to the sample holder with epoxy, a variable displacement is realized as shown in Fig. 5(a). The rest of PEN's surface is freely evolved. The result of simulated in-plane deformation is shown in Fig. 5(a) with a scale factor of 50 to show the deformed shape clearly and the out-of-plane deformation is shown with a color map. Note that since the strain is applied to the PEN through its underside, the free part of the PEN lowers when the nominal strain increases, which can be observed from the color map. One needs to engage the probe to conduct AFM scanning after increasing strain.

Strain local distribution in PEN is also considered. The first principal component of local strain is shown in Fig. 5(b), the axis direction is shown with red arrows and its value is shown with a color map. One can find that the local strain distributes evenly at the center part of PEN, the standard deviation of local strain in the center 2 mm×2 mm square area (size of BFO film) is about 1.3×10^{-4}, which is much smaller than the mean value of local strain.

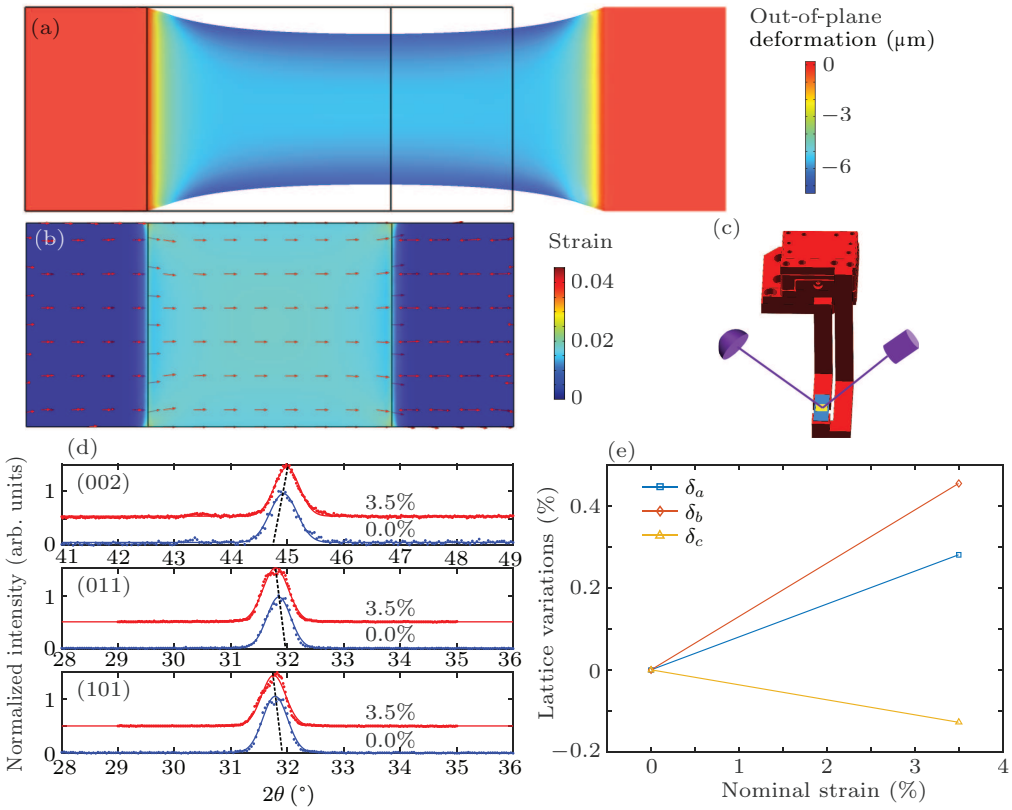


Fig. 5. Strain characterization results. (a) Simulation result of the deformation of PEN under a 3.5% nominal strain. The color map shows the out-of-plane deformation. (b) Simulation result of the strain distribution. Arrows are directions of the first principal axes and the color map shows the first principal component of strain. (c) Scheme of an XRD experiment. (d) XRD diffraction patterns of (002), (011) and (101) planes. Patterns under zero nominal strain and 3.5% nominal strain are plotted, the black dashed lines imply the evolution of strain under stretching. (e) Lattice variations evolution under different nominal strains.

As we mentioned in Section 1, soft matter substrates have been adopted to conduct strain to novel freestanding films.[16,17,23] Since plural issues including the shape of the film, orientation, epoxy curing environment may influence the strain conduction efficiency, calibration is necessary for each sample. XRD is useful for such calibrations, adapters can be utilized to install the sample holder to an XRD set-up, as shown in Fig. 5(c). Take BFO for example, diffraction patterns of (002), (011), and (101) can be measured to calculate the lattice parameters under different nominal strains. One can define lattice variations as

$$\delta_a = \frac{a - a_0}{a_0} \times 100\%, \tag{5}$$

$$\delta_b = \frac{b - b_0}{b_0} \times 100\%, \tag{6}$$

$$\delta_c = \frac{c - c_0}{c_0} \times 100\%, \tag{7}$$

in which a_0, b_0, c_0 are the lattice parameters under zero nominal strain. It has been proven that lattice variations are directly connected to the strain of the film. As shown in Figs. 5(d) and 5(e), from XRD calibrations, we find that the strain is efficiently conducted from the PEN substrate to a freestanding BFO film.

3.2. *In-situ* magnetic imaging

A demonstration of the nano-scale imaging capability of the SNVM is shown in this section. The freestanding BFO film is synthesized on substrate $SrTiO_3$ (STO) and a soluble layer $Sr_3Al_2O_6$ (SAO) with MBE. Then it is transferred to the PEN substrate by solving the SAO layer.[16,17]

The scanning experiment is conducted under ambient conditions and the dual-iso-B protocol is utilized to acquire magnetic signals. A CW spectrum is measured before scanning to decide the MW frequencies to apply. The stray magnetic field B_p is shown in Fig. 6. Be aware that the magnetic pattern is different from epitaxial films,[6,27] this may be due to thermal fluctuations of a freestanding film[28–30] or an epitaxial strain gradient.[31]

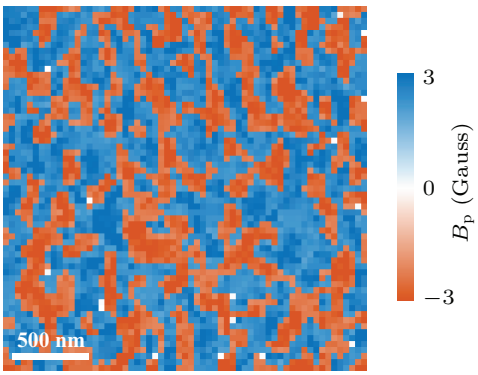


Fig. 6. Real-space scanning result. The stray magnetic field along the NV axis, B_p, is solved from Eq. (4). A mosaic pattern related to thermal fluctuations of freestanding films[23] can be observed.

4. Conclusion

We report an SNVM with *in-situ* strain tuning capability for soft matter. The implementation of the microscope including ODMR data acquiring, AFM scanning control, and microscope head construction is described. The strain distribution on a soft matter substrate is estimated with finite element simulation and an XRD experiment can be utilized to calibrate the strain conduction to a freestanding sample. The capability of nano-scale imaging is demonstrated with an experiment on BFO freestanding film assembled to a soft-matter substrate.

The strain adjuster driven by a linear actuator introduced in this paper can provide arbitrary uniaxial tensile strain. In principle, by upgrading the linear actuator into an actuator system with higher degrees of freedom, the strain adjuster can provide arbitrary in-plane tensile strain. SNVMs equipped with such strain adjusters can help study strain-coupled magnetic physics such as magnetic phase transition under strain,[32] strain-tuned cycloidal orientation,[23] etc.

Because of soft matter's intrinsic low elastic moduli and high ability to bear deformations, the mechanical strain adjuster introduced in this paper is efficient and convenient to tune their strain. By combining the strain-tuning capability with nano-scale magnetic imaging, our SNVM has the potential to analyze the structure of soft matter under adjustable external strain, which is relevant to essential issues in soft-matter science and surface science.[15,18]

Acknowledgements

Project supported by the National Natural Science Foundation of China (Grant Nos. 81788101, T2125011, 11861161004, and 12104447), the National Key R&D Program of China (Grant No. 2018YFA0306600), the Chinese Academy of Sciences (Grant Nos. XDC07000000, GJJSTD20200001, QYZDY-SSW-SLH004, Y201984, and YSBR-068), Innovation Program for Quantum Science and Technology (Grant Nos. 2021ZD0303204 and 2021ZD0302200), the Anhui Initiative in Quantum Information Technologies (Grant No. AHY050000), Hefei Comprehensive National Science Center, China Postdoctoral Science Foundation (Grant No. 2020M671858), and the Fundamental Research Funds for the Central Universities.

The NV scanning probe was provided by CIQTEK and the assembling was completed by Ruige Shao. This work was partially carried out at the USTC Center for Micro and Nanoscale Research and Fabrication.

References

[1] Maze J R, Stanwix P L, Hodges J S, Hong S, Taylor J M, Cappellaro P, Jiang L, Dutt M V G, Togan E, Zibrov A S, Yacoby A, Walsworth R L and Lukin M D 2008 *Nature* **455** 644

[2] Taylor J M, Cappellaro P, Childress L, Jiang L, Budker D, Hemmer P R, Yacoby A, Walsworth R and Lukin M D 2008 *Nat. Phys.* **4** 810

[3] Zhao Z, Ye X, Xu S, Yu P, Yang Z, Kong X, Wang Y, Xie T, Shi F and Du J 2022 *Sub-nanotesla Sensitivity at the Nanoscale with a Single Spin*

[4] Balasubramanian G, Chan I Y, Kolesov R, Al-Hmoud M, Tisler J, Shin C, Kim C, Wojcik A, Hemmer P R, Krueger A, Hanke T, Leitenstorfer A, Bratschitsch R, Jelezko F and Wrachtrup J 2008 *Nature* **455** 648

[5] Tetienne J P, Hingant T, Kim J V, Diez L H, Adam J P, Garcia K, Roch J F, Rohart S, Thiaville A, Ravelosona D and Jacques V 2014 *Science* **344** 1366

[6] Gross I, Akhtar W, Garcia V, Martínez L J, Chouaieb S, Garcia K, Carrétéro C, Barthélémy A, Appel P, Maletinsky P, Kim J V, Chauleau J Y, Jaouen N, Viret M, Bibes M, Fusil S and Jacques V 2017 *Nature* **549** 252

[7] Hedrich N, Wagner K, Pylypovskyi O V, Shields B J, Kosub T, Sheka D D, Makarov D and Maletinsky P 2021 *Nat. Phys.* **17** 574

[8] Wörnle MS, Welter P, Giraldo M, Lottermoser T, Fiebig M, Gambardella P and Degen C L 2021 *Phys. Rev. B* **103** 094426

[9] Dovzhenko Y, Casola F, Schlotter S, Zhou T X, Büttner F, Walsworth R L, Beach G S D and Yacoby A 2018 *Nat. Commun.* **9** 2712

[10] Gross I, Akhtar W, Hrabec A, Sampaio J, Martínez L J, Chouaieb S, Shields B J, Maletinsky P, Thiaville A, Rohart S and Jacques V 2018 *Phys. Rev. Mater.* **2** 024406

[11] Yu G, Jenkins A, Ma X, Razavi S A, He C, Yin G, Shao Q, lin He Q, Wu H, Li W, Jiang W, Han X, Li X, Bleszynski Jayich A C, Amiri P K and Wang K L 2018 *Nano Lett.* **18** 980

[12] Thiel L, Wang Z, Tschudin M A, Rohner D, Gutiérrez-Lezama I, Ubrig N, Gibertini M, Giannini E, Morpurgo A F and Maletinsky P 2019 *Science* **364** 973

[13] Ku M J H, Zhou T X, Li Q, Shin Y J, Shi J K, Burch C, Anderson L E, Pierce A T, Xie Y, Hamo A, Vool U, Zhang H, Casola F, Taniguchi T, Watanabe K, Fogler M M, Kim P, Yacoby A and Walsworth R L 2020 *Nature* **583** 537

[14] Vool U, Hamo A, Varnavides G, Wang Y, Zhou T X, Kumar N, Dovzhenko Y, Qiu Z, Garcia C A C, Pierce A T, Gooth J, Anikeeva P, Felser C, Narang P and Yacoby A 2021 *Nat. Phys.* **17** 1216

[15] Nagel S R 2017 *Rev. Mod. Phys.* **89** 025002

[16] Zang Y, *et al.* 2022 *Adv. Mater.* **34** 2105778

[17] Han L, Fang Y, Zhao Y, Zang Y, Gu Z, Nie Y and Pan X 2020 *Adv. Mater. Interfaces* **7** 1901604

[18] Kavatamane V K, Duan D, Arumugam S R, Raatz N, Pezzagna S, Meijer J and Balasubramanian G 2019 *New J. Phys.* **21** 103036

[19] Badilita V, Meier R C, Spengler N, Wallrabe U, Utz M and Korvink J G 2012 *Soft Matter* **8** 10583

[20] Tokarev A, Yatvin J, Trotsenko O, Locklin J and Minko S 2016 *Advanced Functional Materials* **26** 3761

[21] Lum G Z, Ye Z, Dong X, Marvi H, Erin O, Hu W and Sitti M 2016 *Proc. Natl. Acad. Sci. USA* **113** E6007

[22] Erb R M, Martin J J, Soheilian R, Pan C and Barber J R 2016 *Advanced Functional Materials* **26** 3859

[23] Ding Z, Sun Y, Zheng N, Ma X, Wang M, Zang Y, Yu P, Wang P, Wang Y, Yang Y, Nie Y, Shi F and Du J 2022 *Observation of uniaxial strain tuned spin cycloid in a freestanding $BiFeO_3$ film*

[24] Guo M, Wang M, Wang P, Wu D, Ye X, Yu P, Huang Y, Shi F, Wang Y and Du J 2021 *Rev. Sci. Instrum.* **92** 055001

[25] Jia W, Shi Z, Qin X, Rong X and Du J 2018 *Rev. Sci. Instrum.* **89** 064705

[26] Dréeau A, Lesik M, Rondin L, Spinicelli P, Arcizet O, Roch J F and Jacques V 2011 *Phys. Rev. B* **84** 195204

[27] Haykal A, Fischer J, Akhtar W, Chauleau J Y, Sando D, Finco A, Godel F, Birkhöolzer Y A, Carrétéro C, Jaouen N, Bibes M, Viret M, Fusil S, Jacques V and Garcia V 2020 *Nat. Commun.* **11** 1704

[28] Bakaul S R, Prokhorenko S, Zhang Q, Nahas Y, Hu Y, Petford-Long A, Bellaiche L and Valanoor N 2021 *Adv. Mater.* **33** 2105432

[29] Fasolino A, Los J H and Katsnelson M I 2007 *Nat. Mater.* **6** 858

[30] Ji D, Cai S, Paudel T R, Sun H, Zhang C, Han L, Wei Y, Zang Y, Gu M, Zhang Y, Gao W, Huyan H, Guo W, Wu D, Gu Z, Tsymbal E Y, Wang P, Nie Y and Pan X 2019 *Nature* **570** 87

[31] Sando D, Han M, Govinden V, Paull O, Appert F, Carrétéro C, Fischer J, Barthélémy A, Bibes M, Garcia V, Fusil S, Dkhil B, Juraszek J, Zhu Y, Ma X and Nagarajan V 2020 *Advanced Functional Materials* **30** 2000343

[32] Sando D, *et al.* 2013 *Nat. Mater.* **12** 641